crystals

MDPI

*Article*

# Synthesis and Investigation of $ReSe_2$ Thin Films Obtained from Magnetron Sputtered Re and $ReO_x$

**Kevon Kadiwala [1,*], Luize Dipane [1], Eriks Dipans [1], Arturs Bundulis [1], Martins Zubkins [1], Andrejs Ogurcovs [1], Jevgenijs Gabrusenoks [1], Dmitry Bocharov [1,*], Edgars Butanovs [1,2] and Boris Polyakov [1,*]**

[1] Institute of Solid State Physics, University of Latvia, 8 Kengaraga Str., LV-1063 Riga, Latvia; luize.dipane@cfi.lu.lv (L.D.); eriks.dipans@cfi.lu.lv (E.D.); arturs.bundulis@cfi.lu.lv (A.B.); martins.zubkins@cfi.lu.lv (M.Z.); andrejs.ogurcovs@cfi.lu.lv (A.O.); jevgenijs.gabrusenoks@cfi.lu.lv (J.G.); edgars.butanovs@cfi.lu.lv (E.B.)

[2] Institute of Technology, University of Tartu, Nooruse 1, 50411 Tartu, Estonia

* Correspondence: kevon.kadiwala@cfi.lu.lv (K.K.); bocharov@cfi.lu.lv (D.B.); boris.polyakov@cfi.lu.lv (B.P.)

**Abstract:** The promise of two-dimensional (2D) rhenium diselenide ($ReSe_2$) in electronics and optoelectronics has sparked considerable interest in this material. However, achieving the growth of high-quality $ReSe_2$ thin films on a wafer scale remains a significant challenge. In this study, we adopted a two-step method to produce $ReSe_2$ thin films by combining magnetron sputtering of Re and $ReO_x$ onto flat substrates with subsequent selenization via atmospheric pressure chemical vapor transport (CVT). After analyzing the produced films using X-ray diffraction to identify the crystalline phase in formed thin film and scanning electron microscopy (SEM) to examine surface morphology, it was determined that the suitable temperature range for the 15 min selenization process with CVT is 650 °C–750 °C. Further investigation of these optimally produced $ReSe_2$ thin films included atomic force microscopy (AFM), X-ray photoelectron spectroscopy, and Raman spectroscopy. The bulk electrical analysis of these films and AFM and SEM surface morphology revealed a strong reliance on the type of precursor material used for their synthesis, whereas optical measurements indicated a potential for the films in non-linear optics applications, irrespective of the precursor or temperature used. This study not only provides a new pathway for the growth of $ReSe_2$ films but also sheds light on the synthesis approaches of other 2D transition metal dichalcogenide materials.

**Keywords:** rhenium diselenide; transition metal dichalcogenide; magnetron sputtering; thin films; chemical vapor transport



**Citation:** Kadiwala, K.; Dipane, L.; Dipans, E.; Bundulis, A.; Zubkins, M.; Ogurcovs, A.; Gabrusenoks, J.; Bocharov, D.; Butanovs, E.; Polyakov, B. Synthesis and Investigation of $ReSe_2$ Thin Films Obtained from Magnetron Sputtered Re and $ReO_x$. *Crystals* **2024**, *14*, 690. https://doi.org/10.3390/cryst14080690

Academic Editor: Conrad Becker

Received: 26 May 2024
Revised: 16 July 2024
Accepted: 22 July 2024
Published: 28 July 2024



## 1. Introduction

$ReSe_2$, belonging to the transition metal dichalcogenide (TMD) group, possesses a unique set of properties, including a direct bandgap, high carrier mobility, and robust spin–orbit coupling [1–5]. Unlike group-VI TMDs (molybdenum- or tungsten-based ones), which stabilize in the highly symmetric 2H structure, $ReSe_2$ crystallizes in the 1T triclinic structure (space group $P\bar{1}$ or No 2) with reduced in-plane crystal symmetry [6]. The structure of $ReSe_2$ includes four formula units per unit cell with lattice constants $a$ = 0.6602 nm, $b$ = 0.6716 nm, and $c$ = 0.6728 nm and unit cell angles $\alpha$ = 91.82°, $\beta$ = 104.9°, and $\gamma$ = 118.94°, where the Re-chain direction corresponds to the $b$ axis [7] (Figure A1). Let us separately note that in the published $ReSe_2$ structural studies, different orders of angles and vectors are encountered due to the low symmetry of the structure, making the choice of the order of axes arbitrary. The latest investigations support that $ReSe_2$ has a distorted $CdCl_2$-type structure that is isostructural with a $ReS_2$ compound [3,7,8], rather than a $Cd(OH)_2$-type structure, as was suggested by Alkock and Kjekshus in ref. [9].

This low-symmetry structure gives rise to pronounced in-plane anisotropic optical, electrical, and phonon properties, influencing also thermal conductivity and other vibra-

tional properties, offering considerable promise for creating advanced photonic, electronic, and optoelectronic devices that transcend conventional isotropic 2D materials [4,10–13]. Additionally, the weak interlayer coupling allows $ReSe_2$ bulk to act like electronically and vibrationally decoupled monolayers, resulting in a notable layer-independent nature across various properties [14,15].

The unique structural and electronic properties of $ReSe_2$ extend beyond the realm of electronics, showcasing remarkable catalytic activity for various reactions [16]. Its layered structure provides abundant edge sites, acting as active centers for catalytic processes [17]. Studies reveal its exceptional performance in hydrogen evolution reactions (HERs), offering a promising avenue for clean and sustainable energy generation [17–21]. The multi-layer architecture of $ReSe_2$ is well-suited to energy storage applications. Its interlayer spacing readily accommodates lithium ions, making it a promising candidate for next-generation lithium-ion batteries. Beyond lithium-ion batteries, $ReSe_2$ exhibits potential for supercapacitors, leveraging its excellent charge–discharge rates and long cycle life [22]. These characteristics position $ReSe_2$ as a valuable contributor to the development of efficient and sustainable energy storage systems [22].

Materials with nonlinear optical properties are foundational to the field of nonlinear optics (NLOs), enabling a range of practical applications like optical switching, mode-locking, and optical limiting [13,23]. Optical nonlinearity occurs when a material's characteristics, such as absorptivity and refractive index, change with the intensity of the electric field. Over the years, scientists have discovered a variety of materials in the TMD class that exhibit nonlinear optical properties, with $ReSe_2$ being a notable example [13,23]. The unique attributes of $ReSe_2$, such as its direct bandgap and strong spin–orbit coupling, make it an attractive candidate for cutting-edge NLO technologies, offering researchers and engineers a versatile platform to explore and develop leading-edge optical devices [13,23,24].

In this work, we detail a two-step approach to synthesizing $ReSe_2$ thin films. This study aimed to develop a reliable, scalable method for $ReSe_2$ synthesis. The first step involves magnetron sputtering of $Re/ReO_x$ onto a flat substrate, followed by selenization via atmospheric pressure chemical vapor transport. By comparing films synthesized from both precursor materials—Re and $ReO_x$—we sought to validate the robustness of the methodology and understand how the choice of the precursor impacts various properties of the films. Magnetron sputtering and CVT are both widely used and scalable techniques, suggesting that this method for $ReSe_2$ synthesis holds promise for future scalability. To determine the quality of the structural properties of the synthesized films, comprehensive characterization techniques were utilized for the obtained samples' description. These techniques included X-ray diffraction (XRD) and X-ray photoelectron spectroscopy (XPS) for chemical composition identification, scanning electron microscopy (SEM) for surface morphology analysis, atomic force microscopy (AFM) for detailed surface topography investigation, Raman spectroscopy for vibrational properties characterization, and electrical measurements using the Van der Pauw configuration. Additionally, the optical properties were investigated through transmittance and reflectance measurements, and the nonlinear optical properties were characterized using the Z-scan method.

## 2. Experimental Details

### *2.1. Synthesis of $ReSe_2$ Thin Films*

To find the optimal method for producing high-quality $ReSe_2$ thin films in the framework of this study, we investigated the influence of different precursors (metallic rhenium Re and rhenium oxide $ReO_x$) as well as two substrates: Si (100) wafers with thermally grown 300 nm $SiO_2$ from Semiconductor Wafer, Inc. (Hsinchu, Taiwan) and sapphire (c-plane) from Biotain Crystal Co. (Longyan, China). A two-step approach was employed, starting with the deposition of thin rhenium (Re) and rhenium oxide ($ReO_x$) films with thicknesses ranging between ~10 and 70 nm on both substrates of a ~1 $cm^2$ square (cut by a diamond scriber) size at room temperature by reactive DC magnetron sputtering of a metallic rhenium target (99.9%) in an Ar or mixed $Ar/O_2$ (20 sccm: 10 sccm) atmosphere

($5 \times 10^{-3}$ torr, 100 W DC power)[25]. Prior to the magnetron deposition of the precursor thin films, the substrates underwent a cleaning process. This involved immersing them in an ultrasonic bath with acetone for 3 min, followed by a subsequent 3 min ultrasonic bath in deionized water (DIW). After the ultrasonic cleaning, the substrates were blow-dried using nitrogen ($N_2$) gas to ensure the removal of any residual contaminants. These deposited precursor films served as the foundation for the subsequent conversion to $ReSe_2$ via CVT.

For the CVT process, the configuration of the setup, illustrated in Figure 1c, was operated at atmospheric pressure using a 5% $H_2$/Ar gas mixture. The temperature range tested was from 550 °C to 1000 °C, with a process duration of 15 min (with a pre-heated furnace), and selenium powder (99.99%, Sigma Aldrich, St. Louis, MO, USA) placed at the intake end of the carrier gas. The furnace used here exhibited a temperature gradient, maintaining the target temperature primarily within the central 5 cm region, beyond which, the temperature decreased. Depending on the selected process temperature, the selenium powder was positioned in a zone where the temperature reached 350–400 °C to facilitate its evaporation, to be carried by the flow of the carrier gas to placed samples. A relatively wide range of temperatures was selected to find the ideal temperature range and conduct subsequent, in-depth analyses of the samples produced within the found optimal temperature range.

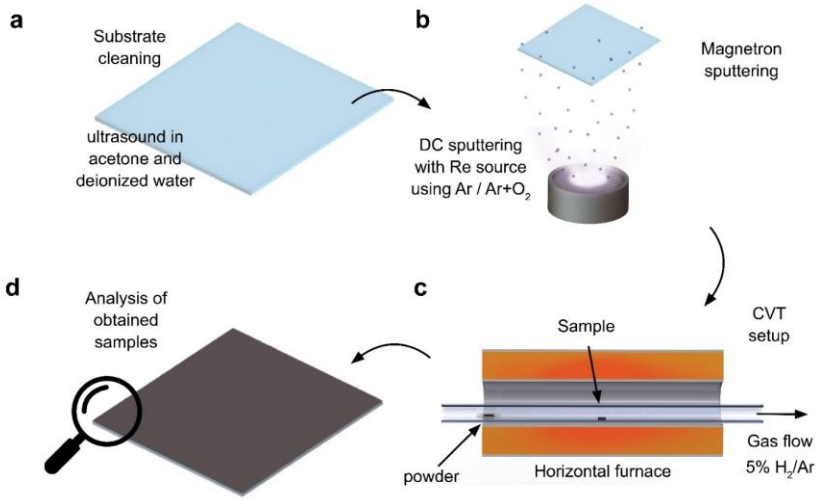


**Figure 1.** Graphical illustration of the methodology followed in this work starting with (**a**) substrate preparation by cutting them in ~10 $mm^2$ square sizes and cleaning them in ultrasound, (**b**) magnetron sputtering of Re and $ReO_x$ precursor films, and (**c**) selenization process at elevated temperatures in horizontal quartz tube CVT setup for 15 min, followed by (**d**) analysis of the synthesized material via various techniques.

### *2.2. Characterization*

High-resolution images of the film surface were obtained using a scanning electron microscope (SEM-FIB Lyra, Tescan, Brno, Czechia) to reveal the morphology and potential artifacts. To further investigate the surface morphology and its electrical profile across the film, experiments were conducted using a PARK NX10 atomic force microscope (Suwon, Korea) in intermittent-contact AFM mode. These measurements employed a platinum cantilever with a tip radius of 30 nm and a setpoint force of 640 nN. The bias voltage applied to the sample was 0.02 V, a value chosen to accommodate the observed conductivity of the samples. Using the same AFM tool, thicknesses of the synthesized $ReSe_2$ films were also measured (Figure 2). During this study, the impact of precursor thickness on selenization was also briefly investigated. Two thicknesses were examined: a thin layer ($\leq$15 nm) and a thick layer ($\geq$50 nm) for both precursors (Re metal and $ReO_x$), as shown in Figure 2 with hatched bars. XRD analysis then confirmed that a 15 min selenization process was of sufficient duration for both the thin and thick precursor materials treated at 650 °C and

750 °C (Figure A2). Following this, all the other chemical, morphological, electrical, and optical characterizations were performed on the prepared thick $ReSe_2$ films.

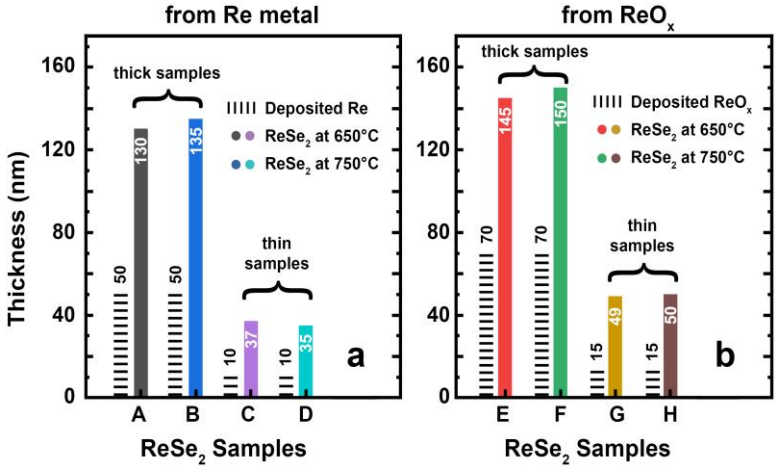


**Figure 2.** Thickness data illustrated here depict the thickness change of the precursor materials (**a**) Re and (**b**) $ReO_x$ when selenized in a CVT setup at 650 °C and 750 °C for 15 min to obtain $ReSe_2$ thin films.

X-ray diffraction (powder diffractometer Rigaku Miniflex 600, Tokyo, Japan) with monochromatic Cu K$\alpha$ irradiation ($\lambda$ = 1.5406 Å) was used to study the phase composition and the patterns obtained were analyzed using PDXL2 software (2.8.3.0 version). Micro-Raman spectroscopy measurements were performed with a 532 nm laser source using a TriVista 777 confocal Raman system (Princeton Instruments, Trenton, NJ, USA) equipped with an upright Olympus microscope with an Olympus UISe MPlanN 100×/0.90 objective and a continuous-wave single frequency. X-ray photoelectron spectroscopy measurements were performed using the ESCALAB Xi (ThermoFisher, Waltham, MA, USA) spectrometer. An Al K$\alpha$ X-ray tube with an energy of 1486 eV was used as an excitation source, the size of the analyzed sample area was 650 µm × 100 µm, and the angle between the analyzer and the sample surface was 90°. The samples were not sputter-cleaned prior to the measurements. An electron gun was used to perform charge compensation. The base pressure during the spectra acquisition was better than $10^{-5}$ Pa.

Furthermore, the electrical resistivity of the produced thin films was measured in the Van der Pauw configuration using a Hall effect system, HMS5000 (Ecopia Hall Effect Measurement Systems, Anyang, South Korea). Four small ohmic contacts at the corners of the samples were made of high-purity silver paint (SPI-PAINT, West Chester, PA, USA). The film's transmittance and reflectance in the range of 330–2500 nm were determined by a Cary 7000 spectrophotometer (Agilent, Santa Clara, CA, USA). The samples were placed at an angle of 6° against the incident beam, and the detector was placed at 180° behind the sample to measure the transmittance and at 12° in front of the sample to measure the specular reflectance. The optical band gap was determined using the Tauc plot for the direct allowed optical transition. It was determined at the energy where the extrapolation of the linear part of the curve intersected with the linear fit of the curve in the energy range of 0.50 to 1.25 eV below the optical absorption edge. In addition, the Z-scan method was employed to characterize the nonlinear optical properties. As the laser source, an ORPHEUS-HP + PHAROS PH2 femtosecond laser with a repetition rate of 500 kHz and pulse width of 150 fs at 900 nm was used. To focus the laser beam, a lens with a focal length of 110 mm was used, resulting in a calculated Rayleigh length of 1.2 mm for this experimental setup.

## 3. Results and Discussion

### *3.1. XRD and SEM Results*

To determine the optimal synthesis temperature for producing $ReSe_2$ thin films using an atmospheric pressure CVT setup, the range of 550 °C–1000 °C was investigated for both precursor materials Re metal and $ReO_x$. $ReSe_2$ peaks are shown in Figure 3 with the obtained XRD patterns. From the XRD patterns, it was found that at a lower temperature (550 °C), the Re metallic precursor did not react completely with selenium. At a higher temperature (1000 °C), the reduction of $ReSe_2$ films was observed for both precursors. This was likely due to the use of a 5% $H_2$/Ar carrier gas mixture, which could be seen from the appearance of the shoulder of metallic Re to the left of the (003) $ReSe_2$ peak. As was estimated by Rietveld refinement performed by Profex code [26] in the sample obtained from the $ReO_x$ precursor films, the reduction of $ReSe_2$ films at 1000 °C was observed to be much more pronounced: the refinement indicated a possible metallic Re phase [27] content of no more than 10% for the sample obtained from Re and a clear presence of the metallic Re phase at 50% and higher for the sample obtained from the $ReO_x$ precursor (see Table A1 for details). Here, it is important to note that in this CVT process, the presence of $H_2$ in carrier gas also boosted the reaction and subsequent selenization rate by producing highly reactive $H_2Se$ gas, and, in addition to this, $H_2$ also played a role in limiting the formation of any undesired oxides while cooling down the synthesized films.

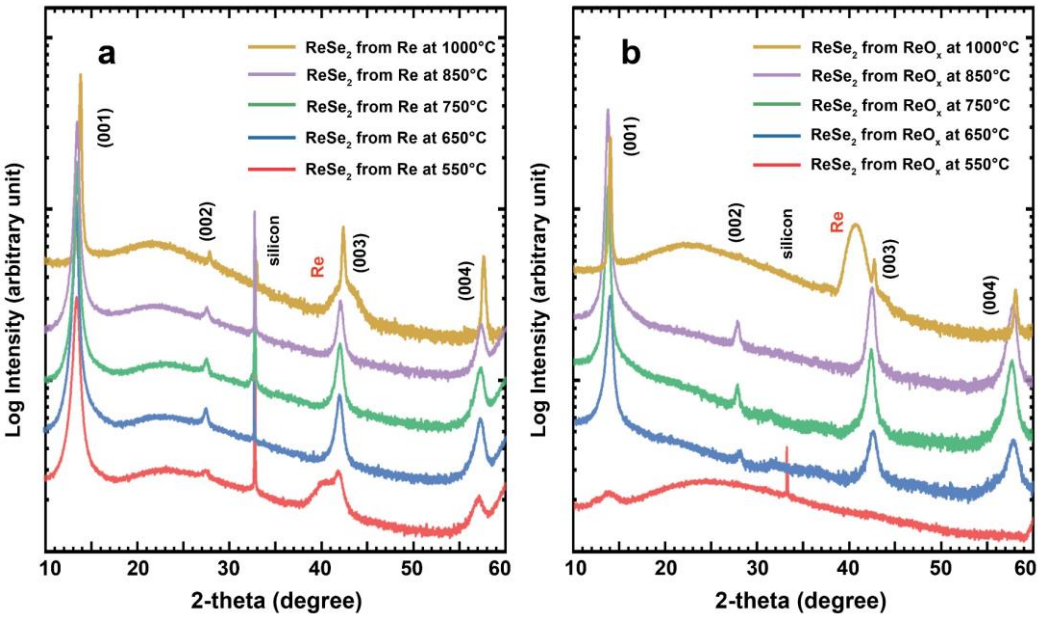


**Figure 3.** X-ray diffraction patterns for the synthesized $ReSe_2$ films from (**a**) Re metal precursor films and (**b**) $ReO_x$ precursor films at 650 °C, 750 °C, 850 °C, and 1000 °C on $SiO_2$/Si substrate for 15 min.

The obtained XRD patterns (Figure 3) matched well with ICDD card no. 04-007-1113 and previous studies conducted on this material [3], indicating the presence of highly crystalline films of $ReSe_2$ in a distorted so-called 1T′ structure with a triclinic symmetry $P\bar{1}$ in the temperature range of 650 °C–850 °C. The Rietveld refinement also confirmed the possibility of the presence of $ReO_2$ [27] and $ReO_3$ [28] phases only in minimal quantities for all samples except the film produced from $ReO_x$ at 550 °C. At the same time, for both series of samples, the Rietveld refinement required pronounced $ReSe_2$ phase reconstruction with lattice constant changes (up to 0.1 Å) and significant atomic shifts in the $ReSe_2$ phase (0.3 Å and more), which were larger for the spectra of samples obtained at high temperatures. This may indirectly have indicated the amorphization of the film or the formation of metallic Re islands at high temperatures or may have been related to the interaction of the film with the substrate and surface effects.

To further investigate the selenization temperatures and their effects on the surface morphology of the produced $ReSe_2$ films, SEM (Figure 4) images were taken. Samples synthesized at lower temperatures were discarded as they showed partially converted precursor materials from the XRD analysis (Figure 3).

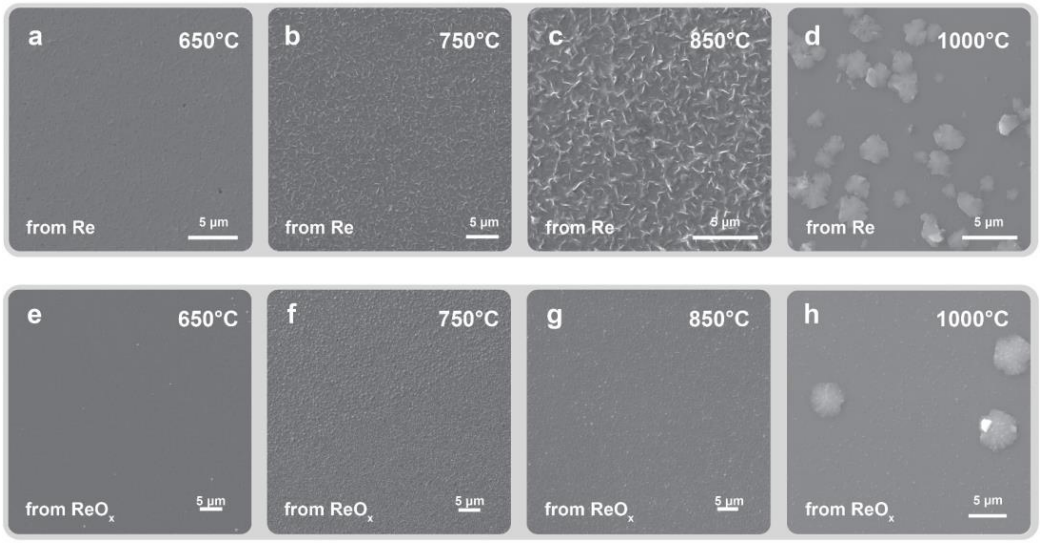


**Figure 4.** SEM images of the synthesized $ReSe_2$ films from (**a**–**d**) Re metal precursor films and (**e**–**h**) $ReO_x$ precursor films using 650 °C to 1000 °C temperatures on silicon as a substrate.

SEM images revealed that as the temperature was increased, surface roughness became more noticeable for both precursors. The films synthesized from the Re metal precursor, which displayed an increase in out-of-plane filamentary structures with increasing temperature and at the highest synthesis temperature tested in this study (1000 °C), particularly displayed a trend of surface crystal formation for films derived from both precursor materials. We hypothesized that the reason for out-of-plane filamentary structure formation in the case of Re precursor-based films could have been due to the high density of the Re metal when it was subjected to such a process (here, selenization), where two extra atoms (Se) were added per one atom of Re; it needed space to expand and when, due to various reasons (interlayer forces), the expansion was restricted, it developed these out-of-plane features to relax the constraining tensions in the film. With the increasing temperature of the selenization, this behavior seemed to become more prominent, resulting in higher density/elevations of these features when compared to lower temperature conversions (Figure 4).

Based on these initial findings, the synthesis temperatures were constrained to two optimal points—650 °C and 750 °C—going forward to study the effects of temperature variation on the synthesized films' properties from different aspects. The samples obtained on a silicon substrate were used to find the optimal synthesis temperature range. Further AFM and optical measurements were performed for the films grown on sapphire only. XRD and SEM analyses confirmed that changing the substrate did not impact the growth process of $ReSe_2$ thin films in the case of using identical synthesis parameters (Figure A3).

### *3.2. AFM Data*

AFM findings (Figure 5) revealed a highly conductive, fine-grained surface, with crystallite sizes typically ranging from 50 to 100 nm, varying with the sample. The AFM topography results (Figure 5a,c,e,g) for $ReSe_2$ films synthesized at 650 °C and 750 °C from Re and $ReO_x$ precursors showed notable differences. At 650 °C, Re-derived films exhibited a rough surface with significant roughness, whereas films from $ReO_x$ presented a more uniform and smoother texture. When the synthesis temperature was increased to 750 °C, the Re-derived films displayed pronounced out-of-plane filamentary structures, indicating

substantial changes in surface morphology, while $ReO_x$-derived films remained relatively smooth but with slightly increased roughness compared to at the lower temperature.

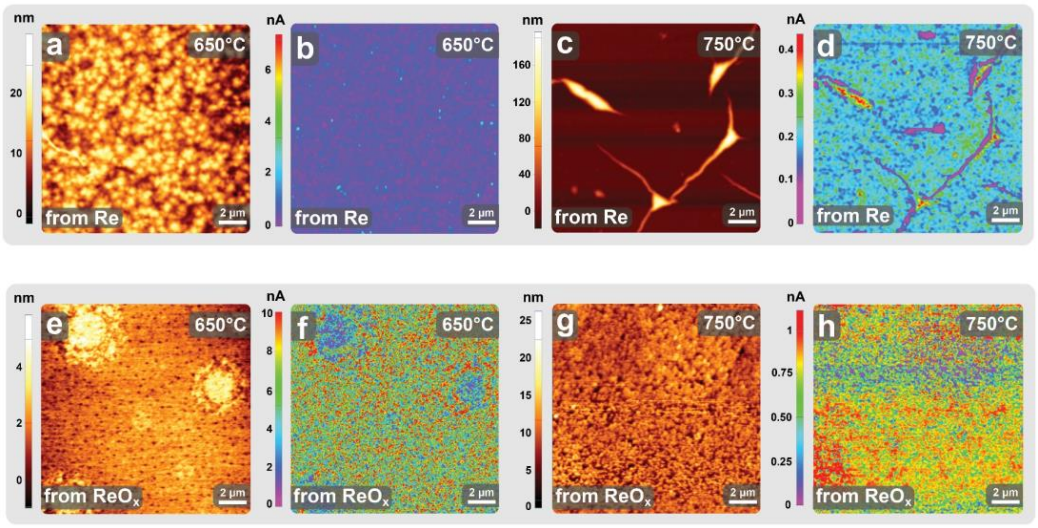


**Figure 5.** AFM images of the synthesized $ReSe_2$ films on the sapphire substrate from the (**a**–**d**) Re metal precursor and (**e**–**h**) $ReO_x$ precursor at 650 °C and 750 °C. (**a**,**c**,**e**,**g**) are topographical images and (**b**,**d**,**f**,**h**) are conductive AFM measurements with platinum tip and 0.02 V bias. All images were taken in a 225 $\mu m^2$ area.

The conductivity mapping results further highlighted the differences in the electronic properties of the films. At 650 °C, the c-AFM mapping for Re-derived films showed a varied distribution of conductivity, corresponding to the rough surface morphology observed. In contrast, the $ReO_x$-derived films exhibited a more homogeneous conductivity map, reflecting their smoother surface. At 750 °C, the Re-derived films continued to show significant variations in conductivity due to their complex surface features, while the $ReO_x$-derived films maintained a more uniform conductivity distribution, consistent with their relatively smoother surface.

These AFM images collectively demonstrate how the precursor material and synthesis temperature influenced the surface morphology and electronic properties of $ReSe_2$ films. Films synthesized from Re metal exhibited more pronounced surface roughness and varied conductivity, particularly at higher temperatures, indicating significant structural and electronic modifications. In contrast, films derived from $ReO_x$ maintained a smoother surface and more uniform conductivity, suggesting a more stable growth process under the same conditions. These findings highlight the importance of precursor selection and temperature control in tailoring the properties of $ReSe_2$ films for specific applications.

### *3.3. XPS and Raman Analysis*

XPS analysis was employed to ascertain the chemical states of the elements in $ReSe_2$ films synthesized from both metal and oxide precursors at 650 °C. The XPS spectra (Figure 6) revealed the presence of only Re and Se elements, alongside organic surface contaminants such as carbon and oxygen. High-resolution spectra of Re 4f and Se 3d peaks were obtained and calibrated against the adventitious C 1s peak at 284.8 eV. The $ReSe_2$ prepared from both precursor types yielded identical XPS spectra. The Re 4f scan exhibited a peak with a single doublet. To minimize error during peak fitting, a spin–orbit splitting $\Delta_{7/2-5/2}$ of 2.43 eV was fixed between the Re $4f_{7/2}$ and $4f_{5/2}$ components of the doublet, with an area ratio of 4:3. The Re $4f_{7/2}$ peak was located at approximately 41.8 eV, indicating a valence state of $4^+$ in the $ReSe_2$ compound. Conversely, the Se 3d peak displayed two doublets (spin-orbit splitting $\Delta_{5/2-3/2}$ = 0.86 eV, area ratio 0.735). The first doublet, with the Se $3d_{3/2}$ at 54.7 eV, corresponded to the 2− chemical state in $ReSe_2$, while the second doublet, with the Se $3d_{5/2}$ at 55.2 eV, suggested the presence of elemental Se on the selenide surface [3,21,29,30].

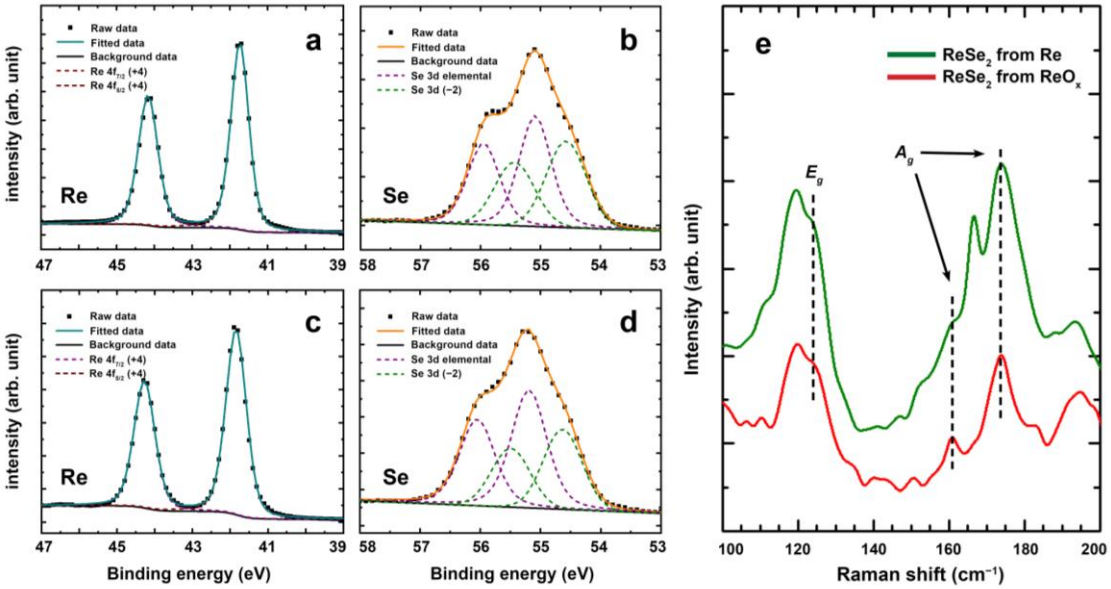


**Figure 6.** XPS spectra of $ReSe_2$ films synthesized at 650 °C from (**a**,**b**) Re precursor films and (**c**,**d**) $ReO_x$ precursor films. (**e**) Raman spectra of the $ReSe_2$ films synthesized at 650 °C measured with a 532 nm wavelength laser. All results were obtained from the films synthesized on the sapphire substrate.

Raman spectroscopy was also employed to further verify the composition and structure of the $ReSe_2$ films synthesized at 650 °C. The Raman spectra (Figure 6e) of these films revealed distinct vibrational modes corresponding to the $E_g$ and $A_g$ modes of $ReSe_2$, aligning well with previously reported studies [10,31]. In this case, the $E_g$ and $A_g$ modes were characteristic of the in-plane and out-of-plane vibrations of the Re and Se atoms in the $ReSe_2$ crystal lattice. The consistency of these Raman peaks with literature values confirmed the successful formation of $ReSe_2$, with the expected crystalline structure and chemical composition.

### *3.4. Optical Measurements*

Figure 7 shows the transmittance, absorbance, and specular reflectance of $ReSe_2$ films synthesized on c-plane sapphire, measured across the spectrum from 500 to 2500 nm. A notable trend emerged, revealing that $ReSe_2$ films synthesized from $ReO_x$ exhibited higher transparency in the infrared region, specifically within the range of approximately 1100 to 2500 nm (Figure 7a). The higher transmittance was attributed to significantly lower absorbance within the relevant spectrum, as depicted in Figure 7b. The observed optical properties demonstrated a clear correlation with temperature-dependent electrical resistivity measurements (Figure 8c), indicating that films produced from $ReO_x$ were semiconductors ($d\rho/dT < 0$), while those from Re exhibited higher conductivity and metallic behavior as a degenerate semiconductor, with a slight increase in resistivity with temperature ($d\rho/dT > 0$) due to increased lattice phonon scattering. Consequently, the pronounced absorbance observed in general was attributed to the higher concentration of charge carriers. The type of conductivity, carrier concentration, and mobility of the samples could not be determined from the measurements due to inconsistent Hall voltages. This inconsistency was caused by either the carrier mobility being too low (<1 $cm^2(Vs)^{-1}$) or the carrier concentration being too high (>$10^{21}$ $cm^{-3}$), both of which fell outside the measurable value ranges of the system, while those from Re exhibited higher conductivity and metallic behavior. The activation energy $E_a$ derived from Figure 8c for the semiconducting films derived from $ReO_x$ was $E_a$ = 92 meV at 650 °C and $E_a$ = 131 meV at 750 °C. The metallic behavior of the $WSe_2$ films produced from the W metal precursor was also observed in a previous study, suggesting a trend in this synthesis methodology [32]. Addi-

tionally, the selenization temperature influenced the optical properties in both cases of $ReO_x$ and Re precursors, with a more pronounced effect noted in the case of $ReO_x$. Figure 7c presents the corresponding specular reflectance of the films. Since reflectance is influenced not only by, for example, charge carrier concentration, but also by surface roughness, a comprehensive interpretation and clear correlation between reflectance and deposition parameters are challenging. However, the more intense reflection observed at >1200 nm in $ReSe_2$ films synthesized from $ReO_x$ at 650 °C compared to 750 °C was related to the lesser roughness, as confirmed by SEM (Figure 4) and AFM (Figure 5) analyses, which increased specular reflectance.

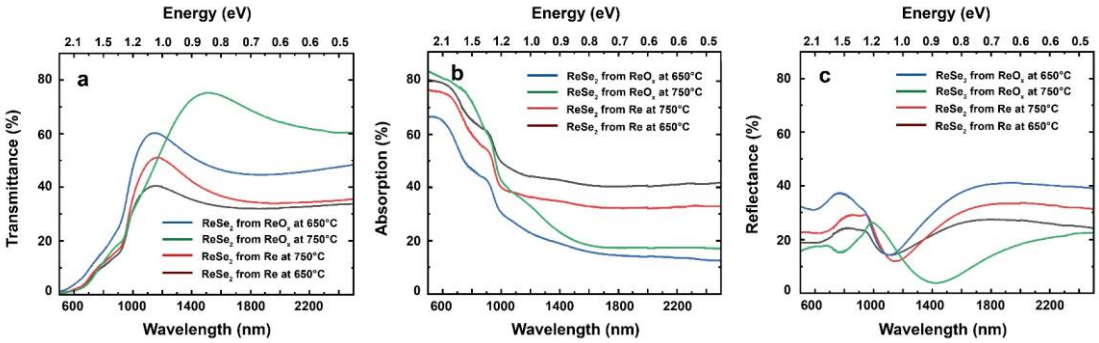


**Figure 7.** (**a**) Transmittance, (**b**) absorption, and (**c**) reflectance of the produced $ReSe_2$ films on the sapphire substrate from both precursor materials in the range of 500–2500 nm wavelength.

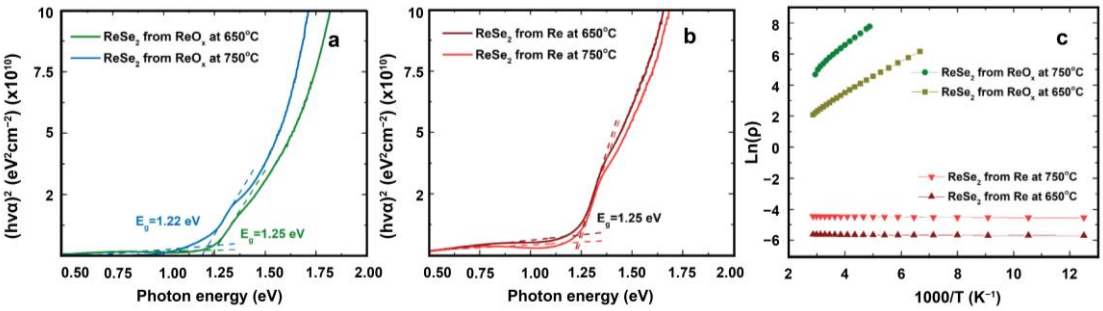


**Figure 8.** Tauc plot to deduce the direct optical bandgap of the $ReSe_2$ films synthesized from (**a**) $ReO_x$ and (**b**) Re metal on the sapphire substrate. (**c**) Arrhenius plot ln(ρ) vs. 1000/T measured using Van der Pauw configuration with a Hall effect system. Used samples for these measurements were covered with $ReSe_2$ films in a 100 $mm^2$ square area on sapphire.

All the as-synthesized films exhibited a dark grey color and were highly absorbed (70–80%) in the visible light range (Figure 7b) due to the small direct optical band gap of approximately 1.25 eV determined from the Tauc plots depicted in Figure 8a,b. These obtained values are consistent with those reported in the literature [13,33].

Furthermore, when using the Z-scan method to assess nonlinear optical properties, the closed-aperture measurements were fitted using a standard Z-scan equation [34]:

$$T_{OA} = 1 + \frac{4 \times \Delta\Phi \times \frac{z}{z_R}}{\left(\frac{z^2}{{z_R}^2} + 9\right) \times \left(\frac{z^2}{{z_R}^2} + 1\right)} \quad (1)$$

where $\Delta\Phi = n_2 \times k \times I \times L_{eff}$ is the induced phase change, $n_2$ is the Kerr coefficient, k is the wave number, I is the optical intensity, $L_{eff} = (1 - \exp(\alpha_0 \times L))/\alpha_0$ is the effective length, $\alpha_0$ is the optical absorption, L is the thickness, z is the sample position, and $z_R$ is

the Rayleigh length. To calculate the nonlinear absorption coefficient from open-aperture data, the following expression was used:

$$T_{CA} = \sum_{n=0}^{\infty} \frac{(\beta \times I \times L_{eff})^n}{\left(\frac{z^2}{z_R{}^2}+1\right)^n \times (n+1)^{3/2}} \quad (2)$$

where β is nonlinear absorption. In the case of absorption saturation, this equation can only be used for low laser intensities ($I < I_s$), in which case, $\beta = -\alpha_0/I_s$, where $I_s$ is saturation intensity [35]. A sample of sapphire substrate was used as a reference measurement. The measured value was $n_2 = (2.16 \pm 0.42) \times 10^{-16}$ cm$^2$/W, which corresponded to values demonstrated in the literature [36]. No nonlinear absorption effect was observed.

A Kerr signal was consistently observed (Figure 9) for all $ReSe_2$ samples synthesized in the suggested optimal temperature range of 650 °C–750 °C, of value $n_2 = (-1.23 \pm 0.65) \times 10^{-2}$ cm$^2$/W, exhibiting minimal variation depending on the preparation procedure. Previous studies of $ReSe_2$/PVA thin films have presented Kerr values at 1560 nm ($n_2 = -2.81 \times 10^{-2}$ cm$^2$/W) [13] and 1900 nm ($n_2 = -6.3 \times 10^{-2}$ cm$^2$/W) [23]. The current findings align with these previous studies and indicate that the Kerr value decreases with wavelength in the infrared region.

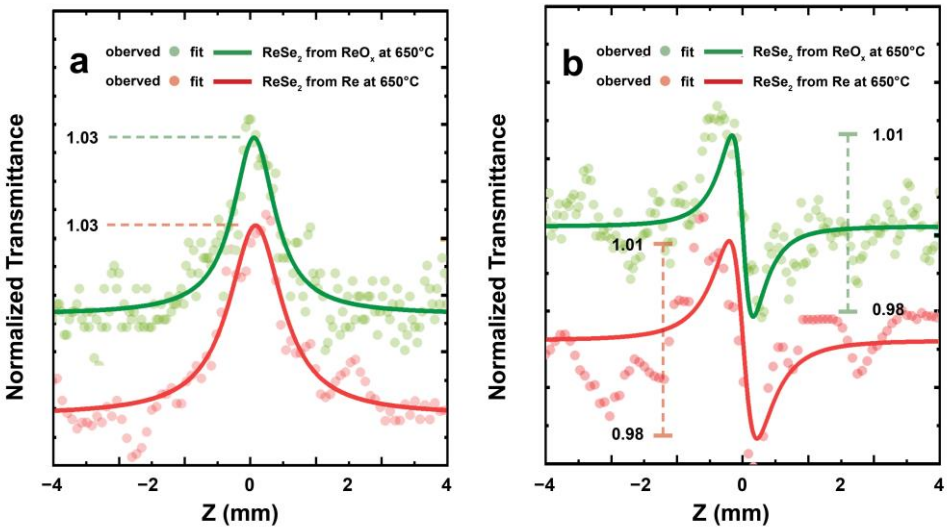


**Figure 9.** Open-aperture measurements of the $ReSe_2$ thin films (**a**) synthesized from Re and $ReO_x$ at 650 °C with a power of 16.4 W and 20.1 W, respectively, and (**b**) open-aperture divided by closed-aperture measurements from Re and $ReO_x$ at 650 °C with a power of 21.2 W and 24.2 W, respectively, and a 900 nm wavelength laser source. All results were obtained from the films synthesized on the sapphire substrate.

Regarding saturation absorption, the value for samples produced from Re was $\beta = (-950 \pm 290)$ cm/GW and for the sample produced from $ReO_x$ it was $\beta = (-730 \pm 330)$ cm/GW. The SA coefficient has been demonstrated to exhibit a dependency on the layer number for $ReSe_2$, ranging from −4156 cm/GW for a single layer (0.71 nm) to −878 cm/GW for 42 layers (bulk sample; 29.81 nm) at 800 nm [24]. The acquired values in this work align well with literature findings for bulk samples. For longer wavelengths, the SA value was measured for the $ReSe_2$/PVA thin films and increased to −5670 cm/GW at 1560 nm [13] and −13,800 cm/GW at 1900 nm [23], indicating an increase in SA values for longer wavelengths. The saturation absorption values of these samples indicated that they could be applicable for Q-switching or mode-locking in laser systems, as 2D materials have been shown to play a key role in ultrafast laser systems [37]. To implement these samples in practice, either samples closer to a few layers (thickness < 7 nm,

as fewer layers lead to higher nonlinearities [24]) or fabricating them in the form of the $ReSe_2$/PVA structure should be considered [13].

## 4. Conclusions

In this study, we synthesized and compared $ReSe_2$ thin films from Re metal and $ReO_x$ precursors deposited using DC magnetron sputtering followed by atmospheric pressure CVT selenization. XRD, Raman spectroscopy, and XPS analyses confirmed the $ReSe_2$ phase for both precursors, with optimal synthesis temperatures between 650 °C and 750 °C. SEM and AFM revealed out-of-plane elongated structures in thin films from the Re metal precursor as the temperature increased, in contrast to the $ReO_x$-derived films. Despite the chemical similarity, the $ReSe_2$ films prepared from Re metal had higher surface roughness, potentially beneficial for catalytic applications such as electrocatalytic HER. Optical properties were largely unaffected by the synthesis temperature, although Re metal films were less sensitive to changes. Non-linear optical measurements showed no significant correlation with synthesis parameters and indicated a potential for the films in non-linear optics applications, such as Q-switching and mode-locking in laser systems. Importantly, semiconductor behavior was observed only in films from $ReO_x$, highlighting the impact of precursor choice on electronic properties and the potential for tailoring material characteristics through controlled synthesis.

**Author Contributions:** Conceptualization, B.P.; methodology, K.K. and L.D.; validation, B.P. and D.B.; investigation, K.K., L.D., E.D., A.O., M.Z., A.B., J.G. and E.B.; data curation, M.Z., A.B., K.K. and B.P.; formal analysis: D.B.; writing—original draft preparation, K.K.; writing—review and editing, E.B. and D.B.; visualization, K.K. and D.B.; supervision, B.P. and E.B.; project administration, B.P. and E.B.; funding acquisition, B.P., E.B. and D.B. All authors have read and agreed to the published version of the manuscript.

**Funding:** This research was funded by the Latvian Council of Science project no. lzp-2022/1-0311. B.P. was supported by the European Union's Horizon 2020 program under grant agreement no. 101087367 (ERA Chair "SWEB"). Support from the European Union's Horizon 2020 program under grant agreement no. 856705 (ERA Chair "MATTER") is greatly acknowledged. The Institute of Solid State Physics, University of Latvia (Latvia), as the Centre of Excellence received funding from the European Union's Horizon 2020 framework program H2020-WIDESPREAD01-2016-2017-Teaming Phase2 under grant agreement no. 739508, project CAMART$^2$.

**Data Availability Statement:** The data that support the findings of this study are included to the paper. Raw-data of measurements is available upon request from the corresponding authors.

**Conflicts of Interest:** The authors declare no conflicts of interest.

## Appendix A

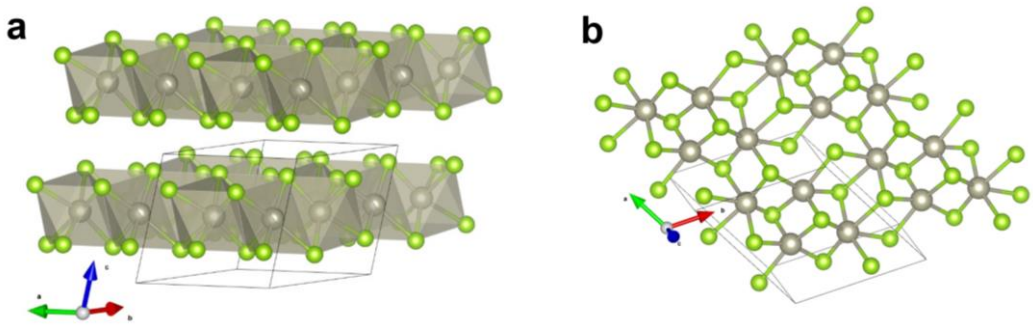


**Figure A1.** Visual representation of 1T-$ReSe_2$ crystal structure. Unit cell is shown with black polyhedral. (**a**) $ReSe_2$ adopts a triclinic crystal system, leading to low symmetry and complex interlayer interactions. Within each layer, the Re atoms (shown in grey color) are in a distorted octahedral coordination, bonded to six Se atoms (shown in green color). (**b**) The Re-chain direction corresponds to the *b* axis (red arrow), but, in different sources, different axis orders are encountered.

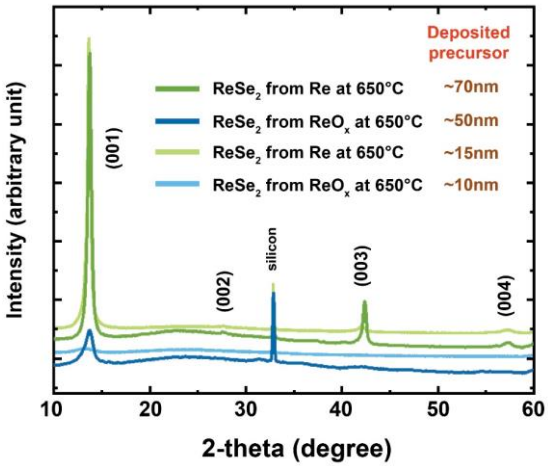


**Figure A2.** XRD patterns of the deposited thin precursor films (~10–15 nm) and relatively thick precursor films (~50–70 nm) converted using 15 min of processing time at the lowest optimal temperature 650 °C.

XRD patterns depicted in Figure A2 validate the selenization process of 15 min at the lowest suggested optimal temperature, which was sufficient for the successful conversion of the deposited precursor up to thicknesses of ~50–70 nm. Using this information, it would be safe to assume that any precursor thickness deposited up to the suggested values would yield high-quality $ReSe_2$ thin films. It is important to note that the measured thickness values for the deposited precursors had a negligible margin of error. However, due to the surface profile variations in the synthesized films of $ReSe_2$, there was a margin of error to consider, ranging from ±5 nm for the smoothest films (low temperature, from oxide) to ±25 nm for the most textured films (high temperature, from metal).

SEM images of $ReSe_2$ on silicon and sapphire substrates shown here in Figure A3 display the similarity of surface morphology behavior present on $ReSe_2$ films grown on both substrates, indicating no significant influence on $ReSe_2$ film growth from the change of substrate. The change of substrate was a necessity due to the need for a transparent substrate in optical measurements, but to maintain the linearity of this study, AFM measurements were also carried out on the films synthesized on the sapphire substrate. Since, neither any electrical nor optical measurements were carried out on the films synthesized on the silicon substrate, it would not be wise to comment on how the change in substrates might affect those properties, but it is also important to remark here that the silicon wafers used in this study had 300 nm of silicon oxide thermally grown on top, which should have passivated any direct influence from the bare Si.

**Table A1.** Estimation of % content of $ReSe_2$, Re, $ReO_2$, and $ReO_3$ in films produced from metallic Re and $ReO_x$ using Rietveld refinement.

| | **From Metallic Re Precursor** | | | | | **From $ReO_x$ Precursor** | | | | |
|---|---|---|---|---|---|---|---|---|---|---|
| Temp. °C | 550 | 650 | 750 | 850 | 1000 | 550 | 650 | 750 | 850 | 1000 |
| $ReSe_2$ | 100 | 99.53 | 99.30 | 98.67 | 92.04 | 76.50 | 94.71 | 96.61 | 88.80 | 28.10 |
| Re | 0 | 0.43 | 0.75 | 0.33 | 7.13 | 3.24 | 3.92 | 2.95 | 7.91 | 71.30 |
| $ReO_2$ | 0 | 0.00 | 0.00 | 0.00 | 0.00 | 15.10 | 0.70 | 0.44 | 2.00 | 0.00 |
| $ReO_3$ | 0 | 0.43 | 0.94 | 0.99 | 0.83 | 5.20 | 0.67 | 0.00 | 1.31 | 0.60 |

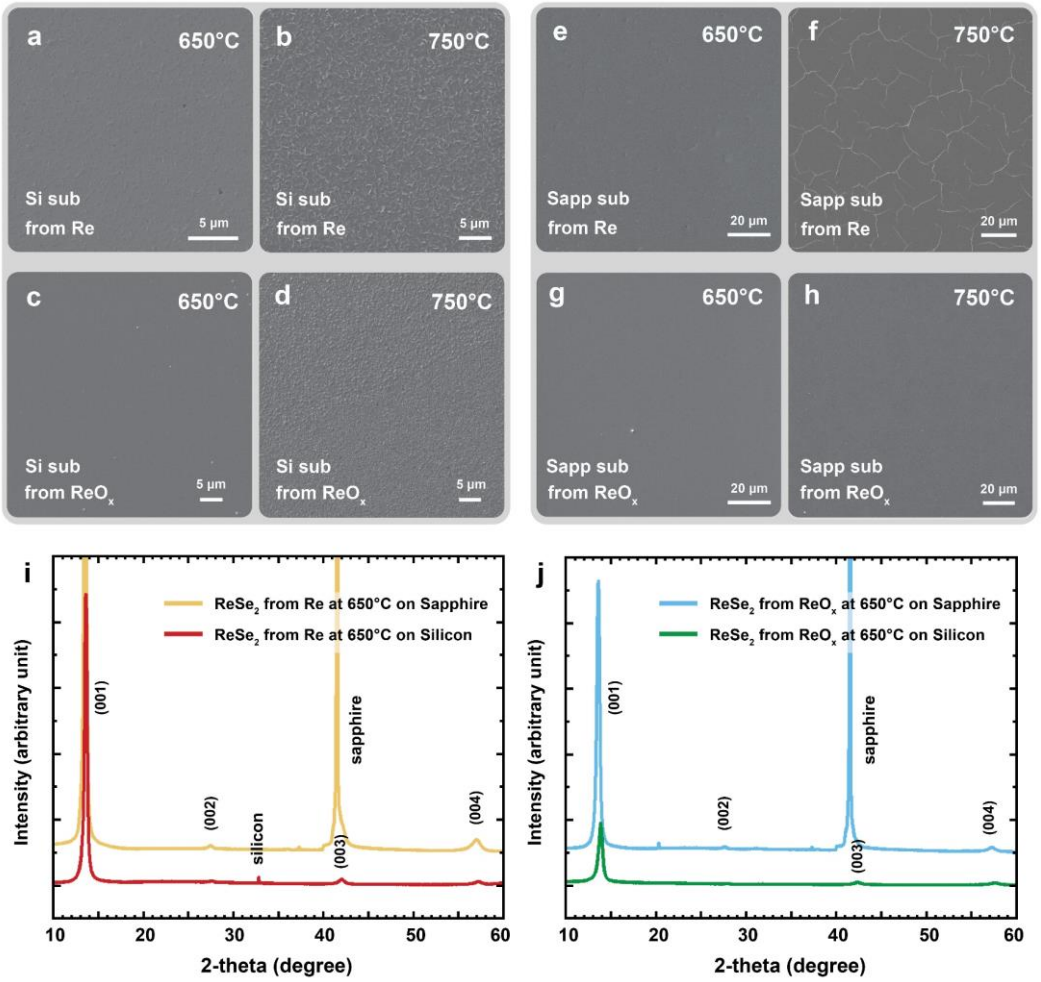


**Figure A3.** SEM images (**a**–**h**) of the synthesized $ReSe_2$ films on (**a**–**d**) silicon substrate and (**e**–**h**) sapphire substrate at 650 °C and 750 °C. XRD patterns of the synthesized $ReSe_2$ films at 650 °C from (**i**) Re metal and (**j**) $ReO_x$ precursor.

## References


1. Wang, C.; Yang, S.; Xiong, W.; Xia, C.; Cai, H.; Chen, B.; Wang, X.; Zhang, X.; Wei, Z.; Tongay, S.; et al. Gate-tunable diode-like current rectification and ambipolar transport in multilayer van der Waals $ReSe_2/WS_2$ p-n heterojunctions. *Phys. Chem. Chem. Phys.* **2016**, *18*, 27750–27753. [CrossRef] [PubMed]
2. Xing, L.; Yan, X.; Zheng, J.; Xu, G.; Lu, Z.; Liu, L.; Wang, J.; Wang, P.; Pan, X.; Jiao, L. Highly crystalline $ReSe_2$ atomic layers synthesized by chemical vapor transport. *InfoMat* **2019**, *1*, 552–558. [CrossRef]
3. Jariwala, B.; Voiry, D.; Jindal, A.; Chalke, B.A.; Bapat, R.; Thamizhavel, A.; Chhowalla, M.; Deshmukh, M.; Bhattacharya, A. Synthesis and Characterization of $ReS_2$ and $ReSe_2$ Layered Chalcogenide Single Crystals. *Chem. Mater.* **2016**, *28*, 3352–3359. [CrossRef]
4. Jiang, S.; Yang, J.; Shi, Y.; Zhao, J.; Xie, C.; Zhao, L.; Fu, J.; Yang, P.; Huan, Y.; Xie, Q.; et al. Salt-assisted growth and ultrafast photocarrier dynamics of large-sized monolayer $ReSe_2$. *Nano Res.* **2020**, *13*, 667–675. [CrossRef]
5. Li, X.; Chen, C.; Yang, Y.; Lei, Z.; Xu, H. 2D Re-Based Transition Metal Chalcogenides: Progress, Challenges, and Opportunities. *Adv. Sci.* **2020**, *7*, 2002320. [CrossRef] [PubMed]
6. Jariwala, B.; Thamizhavel, A.; Bhattacharya, A. $ReSe_2$: A reassessment of crystal structure and thermal analysis. *J. Phys. D Appl. Phys.* **2017**, *50*, 044001. [CrossRef]
7. Wildervanck, J.C.; Jellinek, F. The dichalcogenides of technetium and rhenium. *J. Less Common Met.* **1970**, *24*, 73–81. [CrossRef]
8. Lamfers, H.-J.; Meetsma, A.; Wiegers, G.A.; De Boer, J.L. The crystal structure of some rhenium and technetium dichalcogenides. *J. Alloys Compd.* **1996**, *241*, 34–39. [CrossRef]
9. Alcock, N.W.; Kjekshus, A. The Crystal Structure of $ReSe_2$. *Acta Chem. Scand.* **1965**, *19*, 79–94. Available online: http://actachemscand.org/pdf/acta_vol_19_p0079-0094.pdf (accessed on 22 May 2024). [CrossRef]

10. Wolverson, D.; Crampin, S.; Kazemi, A.S.; Ilie, A.; Bending, S.J. Raman spectra of monolayer, few-layer, and bulk $ReSe_2$: An anisotropic layered semiconductor. *ACS Nano* **2014**, *8*, 11154–11164. [CrossRef]
11. Ran, J.; Chen, L.; Wang, D.; Talebian-Kiakalaieh, A.; Jiao, Y.; Hamza, M.A.; Qu, Y.; Jing, L.; Davey, K.; Qiao, S.Z. Atomic-Level Regulated 2D $ReSe_2$: A Universal Platform Boostin Photocatalysis. *Adv. Mater.* **2023**, *35*, e2210164. [CrossRef] [PubMed]
12. Hart, L.S.; Webb, J.L.; Dale, S.; Bending, S.J.; Mucha-Kruczynski, M.; Wolverson, D.; Chen, C.; Avila, J.; Asensio, M.C. Electronic bandstructure and van der Waals coupling of $ReSe_2$ revealed by high-resolution angle-resolved photoemission spectroscopy. *Sci. Rep.* **2017**, *7*, 5145. [CrossRef] [PubMed]
13. Lee, J.; Lee, K.; Kwon, S.; Shin, B.; Lee, J.H. Investigation of nonlinear optical properties of rhenium diselenide and its application as a femtosecond mode-locker. *Photonics Res.* **2019**, *7*, 984–993. [CrossRef]
14. Liu, F.; Zheng, S.; Chaturvedi, A.; Zólyomi, V.; Zhou, J.; Fu, Q.; Zhu, C.; Yu, P.; Zeng, Q.; Drummond, N.D.; et al. Optoelectronic properties of atomically thin ReSSe with weak interlayer coupling. *Nanoscale* **2016**, *8*, 5826–5834. [CrossRef]
15. Yan, H.J.; Li, Z.; Liu, S.C.; Wang, X.; Zhang, X.; Xue, D.J.; Hu, J.S. Investigation of weak interlayer coupling in 2D layered $GeS_2$ from theory to experiment. *Nano Res.* **2022**, *15*, 1013–1019. [CrossRef]
16. Ndala, Z.B.; Nkabinde, S.S.; Shumbula, N.P.; Makgae, O.A.; Kolokoto, T.; Ek, M.; Gqoba, S.S.; Linganiso, C.E.; Mdluli, P.S.; Moloto, N. Unravelling the Effects of Surface Functionalization on the Catalytic Activity of ReSe2 Nanostructures towards the Hydrogen Evolution Reaction. *Appl. Surf. Sci.* **2023**, *612*, 155971. [CrossRef]
17. Oliveira, C.C.D.; Autreto, P.A.D.S. Optimized 2D nanostructures for catalysis of hydrogen evolution reactions. *MRS Adv.* **2023**, *8*, 307–310. [CrossRef]
18. Zhang, X.Y.; Liu, J.; He, Y.D.; Liu, Z.; Wei, A.X. Synthesis and electrocatalytic performance for hydrogen evolution reaction of $ReSe_2$ nanosheets. *Chalcogenide Lett.* **2022**, *19*, 965–977. [CrossRef]
19. Wang, R.; Han, J.; Xu, P.; Gao, T.; Zhong, J.; Wang, X.; Zhang, X.; Li, Z.; Xu, L.; Song, B. Dual-Enhanced Doping in $ReSe_2$ for Efficiently Photoenhanced Hydrogen Evolution Reaction. *Adv. Sci.* **2020**, *7*, 2000216. [CrossRef]
20. Jiang, S.; Zhang, Z.; Zhang, N.; Huan, Y.; Gong, Y.; Sun, M.; Shi, J.; Xie, C.; Yang, P.; Fang, Q.; et al. Application of chemical vapor–deposited monolayer $ReSe_2$ in the electrocatalytic hydrogen evolution reaction. *Nano Res.* **2018**, *11*, 1787–1797. [CrossRef]
21. Qi, F.; Wang, X.; Zheng, B.; Chen, Y.; Yu, B.; Zhou, J.; He, J.; Li, P.; Zhang, W.; Li, Y. Self-assembled chrysanthemum-like microspheres constructed by few-layer $ReSe_2$ nanosheets as a highly efficient and stable electrocatalyst for hydrogen evolution reaction. *Electrochim. Acta* **2017**, *224*, 593–599. [CrossRef]
22. Ali, H.G.; Khan, K.; Hanif, M.B.; Khan, M.Z.; Hussain, I.; Javed, M.S.; AL-bonsrulah, H.A.Z.; Mosiałek, M.; Fichtner, M.; Motola, M. Advancements in two-dimensional materials as anodes for lithium-ion batteries: Exploring composition-structure-property relationships emerging trends, and future perspective. *J. Energy Storage* **2023**, *73*, 108980. [CrossRef]
23. Lee, J.; Kwon, S.; Kim, T.; Jung, J.; Zhao, L.; Lee, J.H. Nonlinear optical property measurements of rhenium diselenide used for ultrafast fiber laser mode-locking at 1.9 μm. *Sci. Rep.* **2021**, *11*, 9320. [CrossRef] [PubMed]
24. Ge, Y.; Lu, C.; Zhao, Q.; Luo, M.; Liu, Y.; Han, T.; Zhou, Y.; Xu, X. Layer-Dependent Nonlinear Absorption and Refraction of Re $X_2$ (X = Se, S) Films Grown by Chemical Vapor Deposition. *Phys. Rev. Appl.* **2022**, *18*, 034050. [CrossRef]
25. Polyakov, B.; Butanovs, E.; Ogurcovs, A.; Vlassov, S.; Zubkins, M.; Jonane, I.; Cintins, A.; Kalinko, A.; Kuzmin, A.; Purans, J. Understanding the Conversion Process of Magnetron-Deposited Thin Films of Amorphous ReOx to Crystalline $ReO_3$ upon Thermal Annealing. *Cryst. Growth Des.* **2020**, *20*, 6147–6156. [CrossRef]
26. Doebelin, N.; Kleeberg, R. Profex: A graphical user interface for the Rietveld refinement program BGMN. *J. Appl. Crystallogr.* **2015**, *48*, 1573–1580. [CrossRef] [PubMed]
27. Wyckoff, R.W.G. *Crystal Structures*, 2nd ed.; Interscience Publishers: New York, NY, USA, 1963.
28. Dyuzheva, T.I.; Bendeliani, N.A.; Kabalkina, S.S. Compressibility and polymorphism of $ReO_3$ at pressures up to 30 GPa. *Dokl. Akad. Nauk. SSSR* **1988**, *298*, 100–102.
29. Wang, F.; Li, Y.; Shifa, T.A.; Liu, K.; Wang, F.; Wang, Z.; Xu, P.; Wang, Q.; He, J. Selenium-Enriched Nickel Selenide Nanosheets as a Robust Electrocatalyst for Hydrogen Generation. *Angew. Chem.* **2016**, *128*, 7033–7038. [CrossRef]
30. Yang, S.; Ye, W.; Zhang, D.; Fang, X.; Yan, D. Layered double hydroxide derived bimetallic nickel-iron selenide as an active electrocatalyst for nitrogen fixation under ambient conditions. *Inorg. Chem. Front.* **2021**, *8*, 1762–1770. [CrossRef]
31. Zhao, X.; Li, Z.; Wu, S.; Lu, M.; Xie, X.; Zhan, D.; Yan, J. Raman Spectroscopy Application in Anisotropic 2D Materials. *Adv. Electron. Mater.* **2023**, *10*, 2300610. [CrossRef]
32. Kadiwala, K.; Butanovs, E.; Ogurcovs, A.; Zubkins, M.; Polyakov, B. Comparative study of $WSe_2$ thin films synthesized via pre-deposited $WO_3$ and W precursor material selenization. *J. Cryst. Growth* **2022**, *593*, 126764. [CrossRef]
33. Oliva, R.; Laurien, M.; Dybala, F.; Kopaczek, J.; Qin, Y.; Tongay, S.; Rubel, O.; Kudrawiec, R. Pressure dependence of direct optical transitions in $ReS_2$ and $ReSe_2$. *npj 2D Mater. Appl.* **2019**, *3*, 20. [CrossRef]
34. Sheik-Bahae, M.; Said, A.A.; Wei, T.-H.; Hagan, D.J.; Van Stryland, E.W. Sensitive measurement of optical nonlinearities using a single beam. *IEEE J. Quantum Electron.* **1990**, *26*, 760–769. [CrossRef]
35. Koushki, E.; Ara, M.H.M.; Doost, H.A. Z-scan technique for saturable absorption using diffraction method in γ-alumina nanoparticles. *Appl. Phys. B* **2014**, *115*, 279–284. [CrossRef]

36. Major, A.; Yoshino, F.; Nikolakakos, I.; Aitchison, J.S.; Smith, P.W.E. Dispersion of the nonlinear refractive index in sapphire. *Opt. Lett.* **2004**, *29*, 602–604. [CrossRef]
37. Wu, K.; Zhang, X.; Wang, J.; Li, X.; Chen, J. $WS_2$ as a saturable absorber for ultrafast photonic applications of mode-locked and Q-switched lasers. *Opt. Express* **2015**, *23*, 11453–11461. [CrossRef]